

Observational Constraints of Stellar Collapse: Diagnostic Probes of Nature’s Extreme Matter Experiment

Chris L. Fryer* and Wesley Even

CCS Division, Los Alamos National Laboratory, Los Alamos, NM 87545, USA

Brian W. Grefenstette

Space Radiation Lab, California Institute of Technology, Pasadena, CA 91125, USA

Tsing-Wai Wong

*Center for Interdisciplinary Exploration and Research in Astrophysics (CIERA) & Department of Physics and Astronomy,
Northwestern University, 2145 Sheridan Road, Evanston, IL 60208 and*

Harvard-Smithsonian Center for Astrophysics, 60 Garden St., Cambridge, MA 02138, USA

(Dated: April 27, 2022)

Supernovae are Nature’s high-energy, high density laboratory experiments, reaching densities in excess of nuclear densities and temperatures above 10 MeV. Astronomers have built up a suite of diagnostics to study these supernovae. If we can utilize these diagnostics, and tie them together with a theoretical understanding of supernova physics, we can use these cosmic explosions to study the nature of matter at these extreme densities and temperatures. Capitalizing on these diagnostics will require understanding a wide range of additional physics. Here we review the diagnostics and the physics needed to use them to learn about the supernova engine, and ultimate nuclear physics.

I. INTRODUCTION: SUPERNOVAE AS EXTREME-MATTER EXPERIMENTS

Core-Collapse Supernovae are among the most powerful explosions in the universe, produced when the core of a massive star is no longer able to support itself and collapses. The collapse continues until the core reaches nuclear densities at which point nuclear forces and neutron degeneracy pressure halt the collapse. The compression produces densities in excess of nuclear densities and temperatures above 10 MeV. Although laboratory experiments such as PREx [1] might allow scientists to probe properties of the neutron, core-collapse supernova have the potential to probe the broader properties of nuclear matter at densities above nuclear.

Nuclear physics is at the heart of the core-collapse supernova problem. The behavior of matter at nuclear densities determines the depth of the bounce which, in turn, can alter the strength of the bounce shock causing a prompt explosion[2]. Although this prompt explosion mechanism is no longer favored, the behavior of matter at nuclear densities still plays a role in the explosion, defining the neutrino luminosity and spectra, determining the maximum compression of the core and altering the extent of the bounce shock. Similarly, uncertainties in the nuclear reaction rates alter both the explosive and r-process yields in supernovae.

In this paper, we review core-collapse supernovae from the point-of-view of a nuclear physics experiment. As with many laboratory experiments, nuclear physics is

only one piece of the core-collapse supernova problem (see review by Hix et al. in this issue), and all this physics must be understood and/or its uncertainties limited if we are to study any piece of the physics. Fortunately, there are a broad set of diagnostics probing core-collapse supernovae ranging from direct probes of the core limited to only the most nearby supernovae (neutrinos and gravitational waves) to integrated probes that include many objects (nucleosynthetic yields or the mass distribution of compact remnants). But to truly take advantage of this data, theoretical models are critical. New theory models of the progenitors, the supernova engine and its subsequent explosions have been advancing the physics and strengthening our ability to use these diagnostics to probe the physics behind core-collapse supernovae. This approach is not so different than many laboratory experiments. Although experimentalists strive to design an experiment to directly observe the intended physics, most experiments are driven by a wide range of physics and theoretical models are often needed to reduce the uncertainties and interpret the results.

Before we discuss the diagnostics in detail, let’s review the basic supernova engine mechanism and the stages at which the diagnostics help us pin down this engine. We will revisit aspects of this explosion mechanism throughout the paper as they pertain to specific diagnostic probes. The supernova progenitor, a star more massive than $\sim 8M_{\odot}$ progresses through a series of burning phases, building up a dense core. For most pre-supernova progenitors, an iron core is produced that continues to grow until it can no longer support itself, collapsing to form a neutron star. Some super-asymptotic giant branch stars can collapse without forming an iron core, the so-called electron capture supernovae[3]. Supernova progenitors can be observed by searching for the absence of progenitors in survey data after the supernova

* Also at Physics and Astronomy Department, University of New Mexico, Albuquerque, NM 87545; Department of Physics, The University of Arizona, Tucson, AZ, 85721; fryer@lanl.gov

fades and the list of these observed stars has increased steadily over the past decade (see Sec. IV).

The iron core is supported by thermal and electron degeneracy pressure. As the mass increases, the core contracts until electron capture and the dissociation of iron atoms remove both these pressure sources, causing the core to collapse. The compression accelerates the capture and dissociation, leading quickly to a runaway collapse. The collapse continues until the core reaches nuclear densities where neutron degeneracy pressure and nuclear forces halt the collapse, causing the imploding star to bounce. The bounce shock stalls and the current "standard" picture of supernovae argues that convective instabilities (e.g. Rayleigh-Taylor[4], advective-vortical instabilities[5], or advective-acoustic[6]) revive the shock, driving an explosion.

Neutrinos emitted in the core increase during the collapse but, in the extreme densities at bounce can be trapped in the core. As the bounce shock expands, the neutrinos leak out, producing the strong burst of neutrinos and a near-direct probe of the behavior of matter at nuclear densities. The neutrino signal persists as the neutron star cools and can be further enhanced by late-time accretion (caused as material initially swept up in the shock is unable to escape the gravitational pull of the neutron star) onto the supernova. Gravitational waves also probe this core region during the bounce and convective engine time frame, but are more sensitive mass motions caused by rotation and convection. Elements are synthesized in a variety of processes: explosive nucleosynthesis as the shock moves through the silicon layer in the star causing fusion up through iron peak elements, r-process elements produced in winds from the cooling proto-neutron star or from secondary ejecta caused by accretion onto the newly formed neutron star. Measuring these nucleosynthetic yields in stars or asteroids provides another clue into the supernova engine (albeit in an integrated sense).

As the supernova shock breaks out of the star, photons trapped in the shock are also able to leak out. This shock breakout marks the first optical emission from the supernova explosion. The shock continues to expand, producing the bright emission whose details characterize the broad range of Ib, Ic, Iip, IIn, III, I Ib observed supernova classes. Observations of the breakout probes the photosphere of the star, whereas the peak and late-time light curve probe both characteristics of the star (photosphere, circumstellar medium, sometimes mass) as well as the yield of ^{56}Ni .

Supernova remnants, both the compact collapsed cores (neutron stars and black holes) and the ejecta remnants provide further diagnostics of the supernova explosion. Hundreds of years after the explosion, the supernova ejecta is still visible as a remnant. The supernova ejecta remnants provide yet further clues to the explosion asymmetry and nucleosynthetic yields. The mass distribution and spin of compact remnants (the black hole or neutron star formed during collapse) can also provide clues

in understanding the supernova engine. In this review, we study all of these diagnostics. First, we focus on the most direct diagnostics of the nuclear physics: neutrinos (Sec.II) that probe the collapsed core with the neutrosphere touching the surface of the newly-formed neutron star and gravitational waves (Sec.III) that probe the matter motion near the proto-neutron star. We then turn to the more integrated diagnostics. These diagnostics are much more common, but analyzing the data requires much more complex models with integrated physics. To constrain these diagnostics, we must understand the progenitors (Sec. IV) and obtain as much data as possible on the supernova outburst itself including light curves and spectra (Sec. V), the supernova ejecta (Sec. VII), mass distributions of the compact remnants (Sec. VI), and the integrated nucleosynthetic yield estimates (Sec. VIII). As an example of the strength of these combined diagnostics, we review the study of r-process elements from core-collapse supernovae (Sec. IX).

II. NEUTRINOS

In an ideal experiment, we develop direct probes of the physics of interest (in our case, the behavior of matter at nuclear densities). If no additional physics alters our probe (or if we understand that additional physics perfectly), we can measure the experiment's goal physics directly. For our nuclear-physics supernova experiment, neutrinos are that direct diagnostic. The neutrosphere, the surface of last scattering for neutrinos, occurs just above the edge of the proto-neutron star formed in the collapse of a massive star. As such, it provides a detailed probe of the conditions of the core and the behavior of matter at nuclear densities. In addition, understanding neutrino interactions themselves is an important open question in nuclear and particle physics.

A broad set of neutrino detectors sensitive to the $\sim 10\text{MeV}$ neutrinos characteristic of core-collapse supernovae are either operating or under development. These detectors take advantage of a broad set of technologies: liquid scintillation, water Cherenkov, and liquid Argon detectors. A review of the current state of our understanding of neutrinos and current and upcoming neutrino detectors has recently been completed[7]. Here we will briefly summarize this review and then focus on how observations of supernova neutrinos probe nuclear and neutrino physics.

For liquid scintillation detectors, the Borexino[8] and KamLAND[9] detectors continue to operate, SNO+[10] and JUNO[11] experiments are under construction, and the Hanohano[12] and LENA[13] experiments are in the proposal phase. Super-Kamiokande[14] and SNO[15] are the leading water Cherenkov detectors and the Hyper-K (the upgrade to Super-Kamiokande) detector is under research and development. The sheer size of Hyper-K will yield 250,000 interactions from a Galactic supernova, providing a detailed signal ($\sim 250,000$ interactions) to

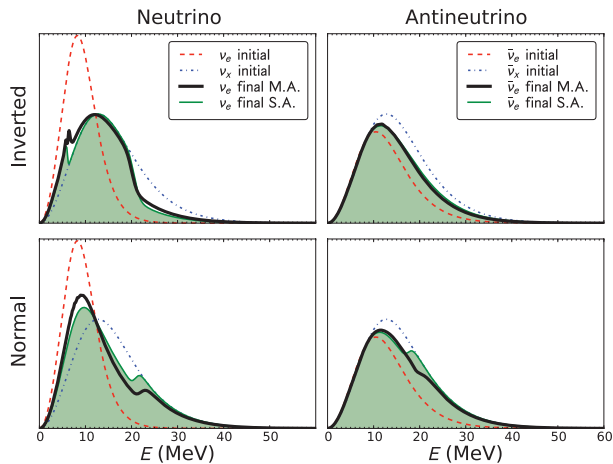


FIG. 1. Spectra of ν_e (left) and $\bar{\nu}_e$ (right) at infinity, for both IH (top) and NH (bottom). Multiangle (M.A.) results are shown with thick solid curves, single-angle (S.A.) with filled regions. Initial spectra are also shown, as marked. Reprinted with permission from H. Duan & A. Friedland, Physical Review Letters, Vol 106, 091101 (2011)[28]

study many nuances of neutrino and nuclear physics (if we can use diagnostics to constrain the progenitor, rotation and aspects of the explosion engine). The Large Baseline Neutrino Experiment is pursuing liquid argon detector technology that will be sensitive to ν_e interactions, probing the physics signatures predicted for these neutrinos.

Supernova probes of neutrino physics include many-body interactions, nuclear correlation effects, mean-field approximations (e.g.[16, 17]). Detections of the neutrinos, especially if we can place constraints on both the neutrino and anti-neutrino spectra, can constrain this physics. These neutrino effects play a role not only in the neutrino heating, but also the nucleosynthetic yields. Coupling neutrino observations with detailed yield analyses (see Sec.IX) will place strong constraints on this physics. Many of these effects can also be studied after the launch of the supernova in the cooling neutron star (e.g.[18, 19]). Neutrinos from material falling back on the newly formed neutron star can alter the late-time neutrino signal from cooling neutron stars, limiting what we can learn from the neutrino signal[31]. Fortunately, we can place constraints on this fallback by using secondary diagnostics. For example, light curve observations constrain both the explosion energy and ^{56}Ni yield. Coupled with theoretical models of the explosion, we can use the light-curve observations to place constraints on the total fallback. The theory models of fallback can, in turn, be tested by the mass distribution of compact remnants (a third diagnostic).

The detection of neutrino oscillations and a non-zero neutrino mass opens up a number of possibilities in neutrino physics. A major focus of the last 5 years has been the study the flavor-state coupling of neutrinos in the core. The high number densities in the core allow

mutual coherent scattering, resulting in many-body flavor evolution[20–28]. Figure 1 shows an example of how the observed neutrino spectra can change in core-collapse supernovae[28]. If we are able to measure a detailed supernova spectrum, we will place strong constraints on this oscillation physics. In addition, these neutrino oscillations will alter the nucleosynthetic yields and, if we can constrain the astrophysical uncertainties, we may be able to use these yields to constrain neutrino physics[29].

The neutrino spectra can also be affected by oscillations in the turbulence behind the outgoing supernova shock and signatures of the Mikheyev-Smirnov-Wolfenstein (MSW) matter effect can be observed in the neutrino spectra (for a recent discussion, see[30]). These oscillations will alter the neutrino spectra and a detailed spectra can be used to better understand the turbulence and physics models for these oscillations. If we can constrain the turbulence physics through other observations (e.g. ejecta remnants - section VII), the neutrino spectrum places a strong constraint on the MSW effect.

Although we will be able to achieve the detailed spectra needed to test theories of neutrino oscillation with a Galactic supernova, what we can learn from supernovae beyond the Milky Way is limited. Hyper-Kamiokande will detect a hand-full of neutrinos, perhaps even out to the Virgo cluster, but probing nuclear or neutrino physics from this sparse signal will be difficult. Even with Galactic supernovae, we must be able to extract the physics from a variety of physics beyond the nuclear and neutrino physics (e.g. hydrodynamics, initial condition uncertainties, etc.). In this section, we discussed three instances where the neutrino signal can tell us more about the physics by including additional diagnostics: using additional diagnostics to constrain the error from fallback accretion, using nucleosynthetic yields to provide early insight into neutrino oscillations, and using ejecta remnants to constrain turbulence in the explosion to better analyze the MSW effect. In this manner, a full suite of diagnostics is crucial to learning physics from supernovae. In the next sections, we review these additional diagnostics.

III. GRAVITATIONAL WAVES

Gravitational waves, like neutrinos, are also nearly direct probes of the central engine behind supernovae. Whereas neutrinos probe the temperature/density conditions, gravitational waves depend more strongly on the matter motion and rotation of the core. Together, these probes provide broad information on the supernova central engine.

Ground-based interferometric gravitational-wave detectors are ideally-suited for the detection of gravitational waves from stellar collapse. With proof-of-concept designs demonstrated in the Laser Interferometric Gravitational-wave Observatory (LIGO) and Virgo detectors, the next generation of gravitational-wave de-

tectors are being developed: advanced LIGO[32], advanced Virgo[32], KAGRA[33]. The improved sensitivity of these detectors coupled with their broader geographic locations will allow gravitational wave detectors in the next decade to observed detailed signals from Galactic supernovae and pinpoint the locations of these supernovae (important if the supernova is obscured).

Gravitational waves are produced when matter is accelerated in a manner to produce perturbations (h_{jk}) in a background spacetime (g_{jk}^b). Typically, scientists estimate the gravitational wave signal using a multipole expansion, assuming the lowest (quadrupole) order piece dominates the signal:

$$h_{jk}^{\text{TT}} = \left[\frac{2G}{d} \frac{d^2}{c^4 dt^2} I_{jk}(t-r) + \frac{8G}{3d} \frac{1}{c^5} \epsilon_{pqj} \frac{d^2}{dt^2} S_{kp}(t-r) n_q \right]^T T, \quad (1)$$

where I_{jk} and S_{jk} are the mass and current quadrupole moments of the source, d is the distance from the source to the point of measurement, G is the gravitational constant, c is the speed of light, $\frac{d^2}{dt^2}$ is the second second derivative with respect to time (t), ϵ_{ijk} is the antisymmetric tensor, and n_q is the unit vector pointing in the propagation direction. Parentheses in the subscripts indicate symmetrization over the enclosed indices and the superscript TT indicates that one is to take the transverse-traceless projection. Note that a signal only occurs if the acceleration of either the mass or current quadrupole moment is non-zero.

A strong signal requires not only the rapid acceleration of a large amount of mass, but the rapid acceleration of the quadrupole moment of that mass. The large masses and accelerations in core-collapse make these supernovae ideal sources of gravitational wave emission. Several reviews exist covering the gravitational wave signals from core-collapse supernovae, e.g.[34], and we will summarize this literature, focusing on what we can learn from gravitational waves and how this diagnostic helps us better understand supernovae and the physics behind supernovae. Gravitational waves in core-collapse can be separated into 4 separate phases: the bounce of the core, the convection above the proto-neutron star (that ultimately drives the explosion, neutrino emission and convective instabilities in the cooling neutron star, and the further collapse to a black hole in those systems whose core masses exceed the maximum neutron star mass.

For most simulations, the strongest gravitational wave signals are produced during the bounce phase of a rotating progenitor star. In extremely rapid rotating cores, the proto-neutron star can form bar mode instabilities or fragment, generating strong, distinct signatures. Albeit unlikely, these are among the strongest core-collapse signals[35].

As the rotating core collapses, rotational support develops a quadrupole moment in the mass distribution that changes radically with time. Figure 2 shows the signal produced for a range of rotating models, comparing fast and slow-rotating models[36]. The fastest ro-

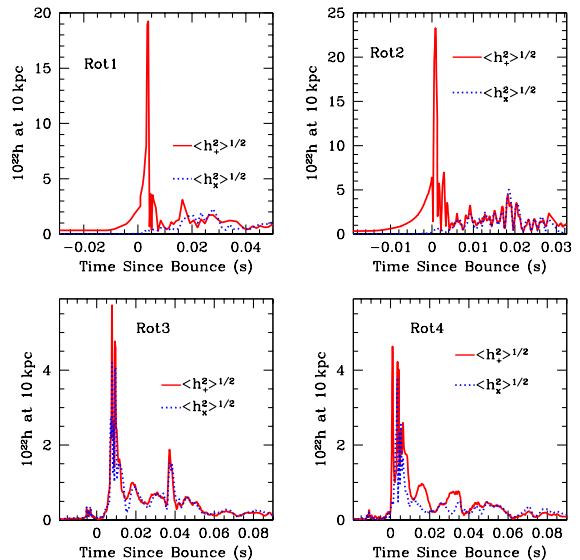


FIG. 2. The angle averaged wave amplitudes ($\langle h_+^2 \rangle^{1/2}$: solid line, $\langle h_x^2 \rangle^{1/2}$: dotted line) for the mass motions from 4 rotating supernova models. Rot2 is the fastest rotating model. Rot3 is what would be predicted for a magnetically braked core. Rot4 shows the signal from the same star as Rot2, but where the rotation was set to zero just before collapse[36]. Note that the gravitational wave signal is a factor of 5 higher in the rapidly versus slowly rotating models. A fast-rotating supernova in the Galaxy should be detectable by advanced LIGO.

tating cores gain enough support from centrifugal forces to alter the peak density achieved at bounce. By measuring the gravitational wave signal, we can determine whether the rotation is fast enough to alter the core densities and hence remove this uncertainty in interpreting the neutrino signal. Currently, the lack of understanding of magnetic braking within stars makes it very difficult for stellar modelers to predict the pre-collapse rotation of stars. Bounce signals will not only allow us to better understand the nuclear physics, but also help constrain stellar models. The amount of rotation can also alter the characteristics of the explosion and there is a synergy between diagnostics measuring the explosion asymmetry: e.g. light curve (sec. V) and ejecta remnants (sec. VII).

After the bounce shock stalls, convection develops both above and below the proto-neutron star surface. Asymmetries in the collapse, caused by explosive silicon burning in the progenitor just prior to collapse, could also produce a strong gravitational wave signal. Figure 3 shows the signals from asymmetric collapse[36]. Typically, large initial asymmetries are required to produce strong signals or alter the peak bounce densities. These signals are distinct from rotating signals and an observed gravitational wave signal will also provide key information on the progenitor evolution (both spin and late-stage burning phases).

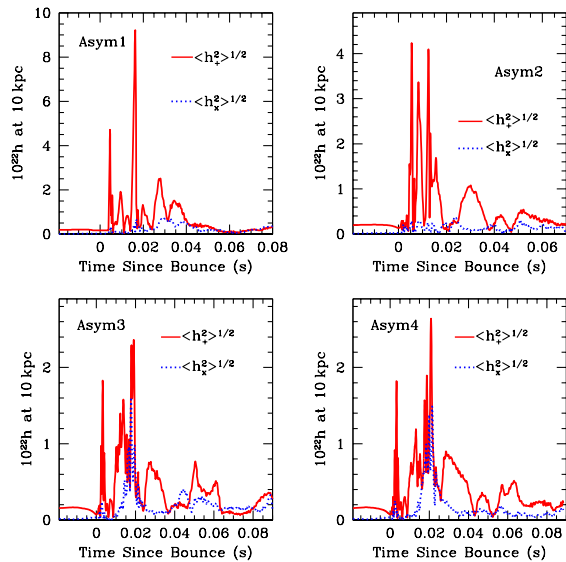


FIG. 3. The angle averaged wave amplitudes ($\langle h_+^2 \rangle^{1/2}$: solid line, $\langle h_x^2 \rangle^{1/2}$: dotted line) for the mass motions from 4 supernovae with global perturbations prior to collapse. Asym1 corresponds to a 25% global perturbation throughout the entire core (assuming oscillatory modes in the neutron star). Asym2 corresponds to a 40% global perturbation in the burning shells only. Asym3 and Asym4 correspond to 30% perturbations in the burning shells, with and without momentum being carried away by neutrinos[36].

Low-mode convection above the proto-neutron star produces rapidly varying quadrupole moments and the resulting emission may also produce a distinguishable gravitational wave signal[37], providing insight into the nature of the convection that we now believe is important for the supernova explosion[4, 5, 38]. This low mode convection produces a specific gravitational wave signature (Fig.4[37]) that can be distinguished from higher mode convection with a sufficiently strong gravitational signature. As we shall see, the distribution of the compact remnant masses may also provide clues into this convective engine and we can test our models against these masses in preparation for any gravitational waves observations (Sec. VI).

Gravitational waves provide probes into 3 key characteristics of the supernova explosion: stellar rotation, bounce asymmetries, and the explosive engine. In all cases, these have ties to the initial progenitor and the explosive engine, and gravitational waves will complement multiple additional diagnostics: progenitor observations (section IV), light-curves (section V), and ejecta remnants (section VII). But gravitational waves suffer some of the same limitations as neutrino diagnostics. Even with the upcoming advanced detectors, gravitational wave detections will be limited to supernova occurring in the local group. We have not yet detected a gravitational wave signature from stellar collapse and,

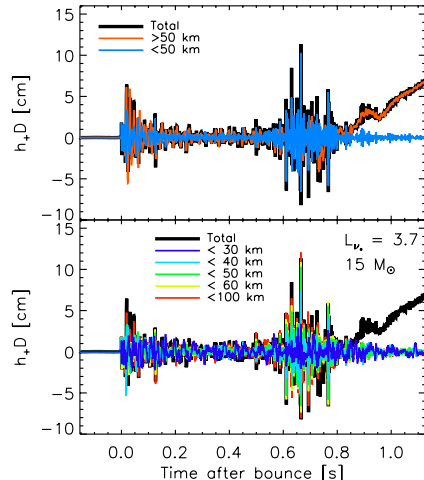


FIG. 4. GW waveforms, $h_+ D$ vs. time, showing the contributions of PNS convection and low mode convection, presumably the Standing Shock Accretion Instability (SASI). For reference, the entire GW signal is shown in both panels (solid-black line). The signal originating from > 50 km (orange, online version) and < 50 km (blue, online version) is shown in the top panel. This radius is roughly the division between nonlinear SASI motions and PNS convection motions. Most, but not all, of the signal associated with prompt convection originates in the outer convection zone. There is a non-negligible contribution from the PNS. The monotonic rise in the GW strain during explosion clearly originates from the outer (exploding) regions. Even though the region for the convection/SASI and its nonlinear motions are above 50 km, these motions influence the PNS convective motions below 50 km. It is telling that once the model explodes, and the nonlinear SASI motions subside but the PNS convection does not, the GW signal from below 50 km diminishes as well. The bottom panel shows the GW signal from five regions, each with different outer radii (30, 40, 50, 60, and 100 km). The strengthening of the GW signal associated with the SASI is apparent for all, suggesting that the influence of the SASI diminishes only gradually with depth. Reprinted with permission from J.W. Murphy, C.D. Ott, A. Burrows, *Astrophysical Journal*, Vol. 707, 1173 (2009)[37].

although it is extremely likely that gravitational wave detectors will observe the mergers of binary neutron star systems in the next 5-10 years (Sec. VI), next generation gravitational wave detectors may be needed to make gravitational wave detections of core-collapse supernovae commonplace events.

IV. PROGENITORS

Without clean, direct probes, the astrophysical problem becomes increasingly complex. We must understand our initial conditions and use a wide variety of diagnostics to better constrain the supernova engine. Astronomers have used supernova rate observations (e.g.[39–42], see [43] for a review), host galaxy environments[44, 45] and massive star populations[46] to help constrain the possible progenitors of supernovae. But such constraints require interpretation from population studies and have had mixed results. For example, one of the basic disagreements in supernova progenitors has been whether the progenitors of type Ib/c supernovae are produced by binaries[46–49] or single stars[50]. Despite extensive observations of both the relative rate of type Ib/c and type II supernovae (and the dependence of the relative rates on the host galaxy metallicity), this remains an open question in our understanding of supernova progenitors. Observations of massive stars may be solving this debate, currently arguing that over 50% of massive stars are in binaries that will interact in their lifetime[51–53], and we will have to understand binary interactions to understand supernova progenitors.

The more reliable constraint on the nature of the progenitor has been direct observations of these progenitors. Observing the pre-supernova star is akin to finding a needle in a haystack. Until large survey archives became available, the only detected progenitors were limited to serendipitous observations at the location of nearby supernovae. These two events, supernova 1993J and 1987A demonstrated just how complex the supernova could be with both being best explained by a binary system where binary interactions shaped the progenitor and circumstellar material, defining many of the supernova features[54]. However, with the Hubble Space Telescope archive, the era of supernova progenitor observations has begun. As future surveys make available their data in archives, the number of progenitor observations should increase dramatically.

Smartt [43] provides an extensive review of the current supernova progenitor database. At that time, surveys had detected 8 new supernova progenitors. From these detections (and analyzed through stellar models), astronomers can estimate the progenitor mass. The Smartt[43] review also includes 12 upper limits that place constraining limits on the upper star mass. Table I summarizes the results from Smartt[42, 43]. The number of progenitor observations continues to grow and table I includes these new systems.

Typically, supernovae with observed progenitors also have detailed observations of the supernova outburst. Coupled with stellar models, we can place constraints on the inner core that then determines the evolution of the collapse and supernova explosion. We will discuss how these constraints can couple with supernova light-curves to understand the progenitor and explosion energy in Sec.V. From the table, we see that most supernova pro-

TABLE I.

Name	Mass
Serendipitous	
SN1987A	14-20 M_{\odot}
SN1993J	$\sim 15M_{\odot}$
Gold Set	
SN2003gd	6-12 M_{\odot}
SN2005cs	6-10 M_{\odot}
SN2008bk	7.5-9.5 $M_{\odot} \rightarrow 11.2-14.6M_{\odot}$ [55]
SN2004dj	12-20 M_{\odot}
SN2004am	9-19 M_{\odot}
Silver Set	
SN1999ev	15-18 M_{\odot}
SN2004A	7-12 M_{\odot}
SN2004et	8-14 M_{\odot}
Bronze Set	
SN1999an	<18 M_{\odot}
SN1999br	<15 M_{\odot}
SN1999em	<15 M_{\odot}
SN1999ev	12-22 M_{\odot}
SN1999gi	<14 M_{\odot}
SN2001du	<15 M_{\odot}
SN2002hh	<18 M_{\odot}
SN2003ie	<25 M_{\odot}
SN2004dg	<12 M_{\odot}
SN2005cs	6-10 M_{\odot}
SN2006my	<13 M_{\odot}
SN2006ov	<10 M_{\odot}
SN2007aa	<12 M_{\odot}
SN2008bk	8-12 M_{\odot}
New	
SN2008ax	10 – 14 M_{\odot} or $\sim 28M_{\odot}$ [56]
SN2008cn	13 – 17 M_{\odot} [57]
SN2009md	7 – 15 M_{\odot} [58]
SN2011dh	13 – 22 M_{\odot} [59–61]
SN2012aw	$\sim 17 – 18M_{\odot}$ [62]
iPTF13bvn	$\sim 31-35M_{\odot}$ [63, 64]

genitors appear to be stars below 20 M_{\odot} . This matches predictions by core-collapse models[65, 66] where strong supernovae are produced on in stars with masses below $\sim 18 – 23M_{\odot}$ (massive stars can still produce strong supernovae if they experience sufficient mass loss to alter the core).

Also note that roughly half of stars have masses below $\sim 12M_{\odot}$. For initial mass functions (IMFs) lying between 2.35 and 2.7 and upper and lower limits of supernova formation ($M_{\text{SNupper}} = 20M_{\odot}$, $M_{\text{SNlower}} = 8 – 10M_{\odot}$), the fraction of supernovae below $\sim 12M_{\odot}$ is expected to lie between 36-63% of all stars. As we build up the statistics on this result, we may be able to place constraints on the lower mass limit for supernovae and the stellar models that predict this limit.

Progenitor observations place constraints on the initial conditions that help us take advantage of all other diagnostics. The constraints on the collapsing core strengthen what we can learn from neutrinos (section II), gravitational waves (section III) as well as our theoretical models so that we can produce more reliable explosion energies

(important for all diagnostics). Constraints on the circumstellar medium also reduce the uncertainties in the light-curve calculations (section V).

But these results must be taken with some caution. For example, new observations of the reddening for the progenitor of SN 2008bk (one of the gold set from Smartt et al.[43]), suggests that the progenitor was highly reddened, altering the mass prediction for the progenitor star for this supernovae[55]. This demonstrates that even our best progenitor masses in the current list are not set in stone. The growth of this data is placing new mandates on stellar evolution models and, with these improvements, we will be able to place stronger constraints on supernova progenitors. With new surveys and broader attempts at archiving these surveys, the rate of supernova progenitor detection is expected to increase dramatically in the next decade. Coupled with supernova light-curves, these observations help identify the initial conditions of our nuclear-physics, astrophysics-laboratory experiment.

V. SUPERNOVA LIGHT-CURVES

Supernovae were first discovered by their transient optical emission and it is not surprising that most of our data on supernovae is concentrated in these bands. With transient observatories (both on ground and in space), the bandwidth for which we have coverage of supernovae now extends from the radio up to the gamma-ray. This broader range, in particular the opening up of the UV and X-ray bands from the Swift[67] and now NuSTAR[68] satellites, has allowed astronomers to probe the interaction of the supernova shock with the circumstellar medium. Recent transient surveys, like PanStarrs and PTF are providing a wealth of new data in the optical bands, including many peculiar transients and more complete light curves with observations well before peak. These early observations have led to a growing list of supernova observations covering very early times when the supernova shock breaks out of the stellar photosphere.

Many studies of supernovae have focused on using the peak brightness to infer the explosion energy, progenitor mass and ^{56}Ni yield. For many type Ia supernova progenitors, where we have already constrained the explosion to a near-Chandrasekhar massed white dwarf with low-density surroundings, such interpretations may be successful. But for the massive stars producing core-collapse supernovae, mass loss (via winds, explosive ejections or binary interactions), the circumstellar medium can drastically alter the light curve. In massive stars, the peak of the light-curve may have nothing to do with the yield of ^{56}Ni yield. Figure 5 shows 3 different light curves for a GRB-associated supernova, where the amount of energy deposited by ^{56}Ni decay is varied by a factor of 100[69]. This is equivalent to reducing the amount of ^{56}Ni produced without changing any other aspect of the explosion. In this case, the peak light-curve is brighter with less energy deposition from ^{56}Ni decay. This is because

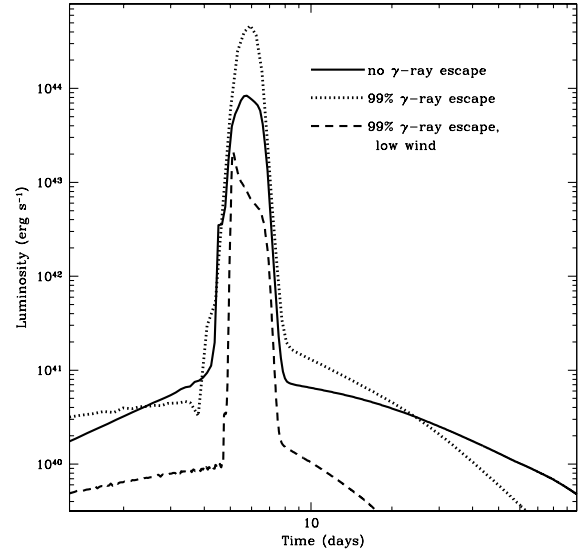


FIG. 5. Luminosity versus time for 3 supernova models using the same progenitor and explosion energy, but varying the amount of energy deposited from ^{56}Ni decay[69]. If decay energy dominated the light-curve, by reducing the amount of energy deposited, we'd expect a dimmer supernova. In fact, the opposite is the case. In this study[69], the focus is on the energy lost because the γ -rays did not interact with the stellar ejecta, but this is equivalent to lowering the total ^{56}Ni in the explosion. However we do see that, because shock heating dominates, the amount of wind material does change the light-curve.

shock heating dominates the light curve at peak.

Realizing that shock heating is an important contributor to the light-curves of many supernovae alters what we can potentially learn from these supernovae. Instead of measuring the amount of ^{56}Ni produced, observations of supernovae are more sensitive to, and can help constrain, the circumstellar medium. For massive stars, the radius where the star ends is difficult to measure as the photosphere is often in the wind or other circumstellar ejecta. The supernova light-curve provides extensive information about this circumstellar medium and the winds/outbursts from stars prior to their collapse. One of the most clear-cut ways to measure this photosphere is through shock breakout. The duration and peak of the shock breakout can measure the radius of the photosphere. For example, figure 6 shows the shock breakout light-curves for a single progenitor and explosion where the mass of the hydrogen envelope has been reduced in two ways: removing the top layers of the hydrogen envelope (in this manner, the radius decreases with the decrease in mass) and reducing the envelope density (in this case, the photospheric radius decreases only slightly with decreasing mass). The time of the shock breakout is most sensitive to the stellar radius, but the density in the giant can also alter the breakout time. Without a

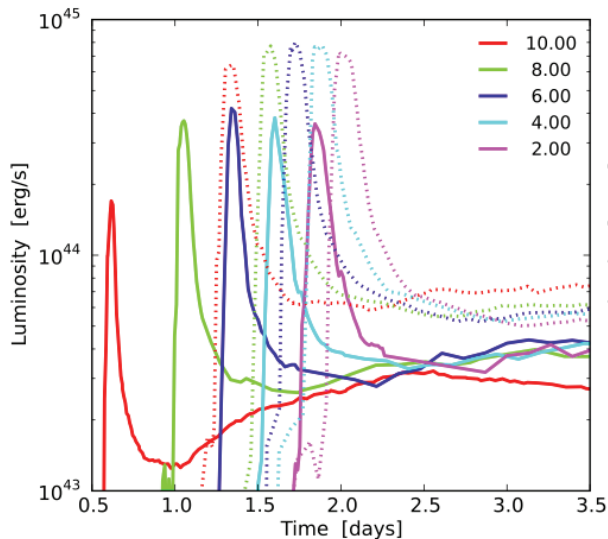


FIG. 6. Bolometric light-curves for shock breakout for a suite of models. The first set (solid lines) shows the breakout for 5 models, each removing a different amount of mass from the hydrogen envelope. For these models, the outer layers of the star are removed in the mass and the mass removal reduces both the envelope mass and the star’s radius. In the latter set (dotted lines), the density of the envelope is lowered, removing mass but not removing radius. Although there is some degeneracy in these model results, in general the mass removal that also reduces the radius has a more drastic effect on the breakout time and duration of breakout[70].

neutrino signal, it may be difficult to pinpoint the exact explosion time, so the width of the shock breakout will play a stronger role in constraining the progenitor characteristics. As surveys begin to probe shorter and shorter transients, shock breakout observations will become increasingly common and these probes of the stellar photosphere will become strong constraints on the supernova progenitor.

Post breakout Supernova light-curves and spectra further probe the circumstellar medium, studying the outbursts and wind ejecta from a supernova progenitor prior to collapse. An extreme example of this is SN 2010jl. In this supernova, interaction with nearly $10 M_{\odot}$ of circumstellar medium kept the supernova bright (even in the X-rays) for over a year after the explosion[71]. Observations of the light-curve allowed astronomers to probe the characteristics of this ejecta, arguing for extreme mass loss immediately prior to the explosion and extremely energetic explosions (either a hypernova or pair-instability supernova). Figure 7 shows a suite of models with the same progenitor and explosion characteristics and varying only the details of the massive circumstellar medium. With these models, we find that SN2010jl can only be explained using a large amount of circumstellar material (over a few M_{\odot}) and an energetic explosion (either a pair-instable supernova or hypernova). If this is a pair-instability supernova, the sur-

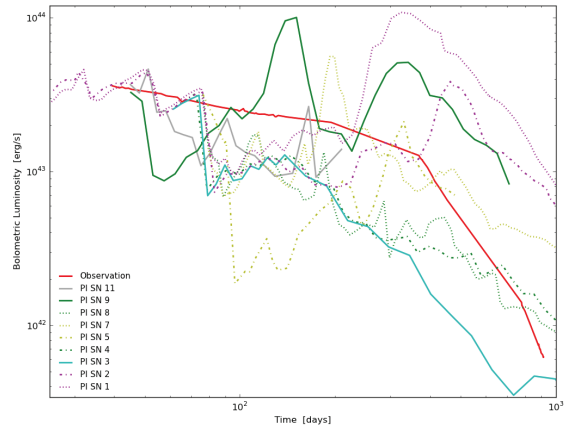


FIG. 7. The light curve in r-band of the SN2010jl supernova[71] coupled with a series of models striving to replicate this effect. These models include a range of pair-instability models, although hypernova models could also be designed to match this data. In any event, all models required considerable envelope mass and explosion energy to explain the extended light curve. We expect high mass loss in both pair-instability and hypernova models so both the energy requirements and circumstellar mass point to these massive explosions.

rounding ejecta demonstrates that pair-pulsations (explosive outburst produced when pair production causes an implosion and resulting explosive burning phase in a star) can occur before the final outburst. Although there is some evidence supporting the existence of these theoretically-predicted pair-instability pulsations and explosions in other observations, this might be the strongest evidence for pair-pulsations and explosions in our current data suite. In this case, the supernova light-curve could place constraints on both the supernova energy and surrounding medium.

Late-time observations of the ^{56}Ni decay curve will still provide insight into the total ^{56}Ni yield. With an adequately developed theory, the wide breadth of supernova light-curve and spectra data that spans from radio up through gamma-rays can be used to not only probe the circumstellar medium and supernova progenitor, but also the characteristics of the supernova explosion (energy and, ultimately explosion asymmetry).

Theory advances are needed to take advantage of this data. Modeling core-collapse light-curves ultimately will require full radiation-hydrodynamics calculations. Solving this correctly requires a 6 dimensional calculation modeling the energy structure, angular distribution and spatial distribution of the photons. To date, most radiation hydrodynamics calculations use simplified transport algorithms (flux-limited diffusion with gray or few groups[72, 73]) in 1-dimension although higher-order transport to follow the angular distribution is technically feasible, it is typically too costly to be implemented in full parameter studies[73]. Those calculations with higher-order transport typically do not couple the radiation to

the hydrodynamics[74, 75]. On top of this, the treatment of opacities often assumes local thermodynamic equilibrium, when the atomic physics suggest that out-of-local thermodynamic equilibrium, perhaps even non-steady state physics is important. Again, codes modeling this physics more accurately tend to not model radiation-hydrodynamics[76]. Research in atomic physics is also important.

These physics uncertainties and numerical obstacles might make it seem that using supernova light-curves and spectra to constrain the supernova engine is a daunting affair. But the rise in data and computational resources will probably make this diagnostic one of the most powerful in the next decade. Coupled with observations of the progenitor as an independent diagnostic, supernovae are ideally suited to test the transport and atomic physics theory. Here, the astrophysics “experimental” community and the high-energy density laboratory community can be very complimentary to each other. Laboratory experiments will also provide insight, ultimately pinning down this physics[77]. As a transport physics experiment alone, supernovae are quite useful. But as this physics is solved, supernova light-curves will also be a strong constraint in understanding supernova progenitors and the supernova explosion. With these constraints, we can approach our studies of nuclear physics with a better understanding of our supernova experiment.

VI. COMPACT REMNANTS

Compact remnant masses place constraints both on the equation of state directly and on the nature of the supernovae explosions mechanism. Equations of state make predictions for the maximum mass of a neutron star. The observed maximum mass places a lower limit on this maximum neutron star mass. The measurement of a $2M_{\odot}$ neutron star[78] has already placed strong constraints on the nuclear equation of state[79]. If this maximum mass pushes upwards either through a new observation or firmer constraints on existing neutron star mass estimates, severe constraints can be placed on the nuclear equation of state at both sub- and supranuclear densities.

The mass of the compact remnant can also provide clues into the explosion mechanism. By using orbital characteristics, the masses of compact remnants in binaries are fairly well constrained and the mass distributions of compact remnants have been estimated by a number of groups[80–85]. Initial mass distributions argued for bimodal, nearly delta-function, peaks. With time, some of these peaks have filled in, but a gap in the masses between the most massive neutron star ($\sim 2M_{\odot}$) and the the lowest mass black hole ($\sim 5M_{\odot}$) persists[81, 83, 84]. However, note that it has been argued that the mass gap could be an artifact in deriving orbital inclination angles of black hole X-ray binaries, which were used in determining the mass functions of black holes[86]. Here we review how the exact nature of this gap provides clues

into the supernova engine.

The observed compact remnant masses are determined by 3 factors: the mass at explosion (depending on the explosion timescale), the amount of fallback after the launch of the shock (dependent on the explosion energy and asymmetry), and long-term accretion from binary companions. For many cases, the binary accretion is small or can be estimated[87, 88]. In such cases, the compact remnant mass distribution can be used to constrain the nature of the supernova explosion.

To discuss this in more detail, let’s review the aspects of the supernova explosion mechanism that affect the compact remnant mass. The bounce shock moves out through the star until neutrino cooling, and to a lesser extent, dissociation of the infalling silicon layer, sap its energy and it stalls. The region between the proto-neutron star surface and the stalled shock is susceptible to a number of instabilities. Much of the early work focused on Rayleigh-Taylor instabilities in this stalled shock region[4, 89–92]. If these are present, they tend to dominate. If the Rayleigh-Taylor instability is weak, additional instabilities can develop and dominate. Early papers invoking the “Standing Accretion Shock Instability” focused on new instabilities, e.g. the advective-acoustic instability[5, 93–95].

The Compact remnant mass distribution is able to provide insight into which instability dominates, and therefore determine the exact conditions of the explosion. The advective-acoustic instability has a growth time that is > 10 times longer than Rayleigh-Taylor. This longer growth time tends to produce delayed explosions taking $\sim 0.5 - 1$ s to develop[5], in contrast to the 100-200 ms explosions produced in simulations with strong Rayleigh-Taylor convection[65]. Measuring the delay could potentially constrain the explosion engine[96].

The duration of the explosion is not just important in determining the neutrino signal. A sufficiently detailed neutrino signal could both measure the explosion duration and neutrino physics effects. But it is more likely that the next neutrino measurement will be pushing the limits of detectability and the signal will be limited to just a handful of detections. For this, having an alternate measurement of the delay will help us take full advantage of the neutrino signal. If we assume that the convection region dominates the explosion energy, a good estimate of the explosion energy can be made by setting the energy stored in this region when the explosion occurs and the shock is launched. This energy, in turn, depends upon the accretion rate of the infalling star onto this convective region[96, 98]. With these assumptions, we can estimate the explosion energy as a function of time, shown in figure 8.

Assuming a fraction of the explosion energy goes toward unbinding the star, one can estimate the amount of fallback in the system, predicting a final remnant mass. In this manner, we can estimate the compact remnant mass as a function of initial stellar mass[96]. Including population synthesis calculations, one can estimate the

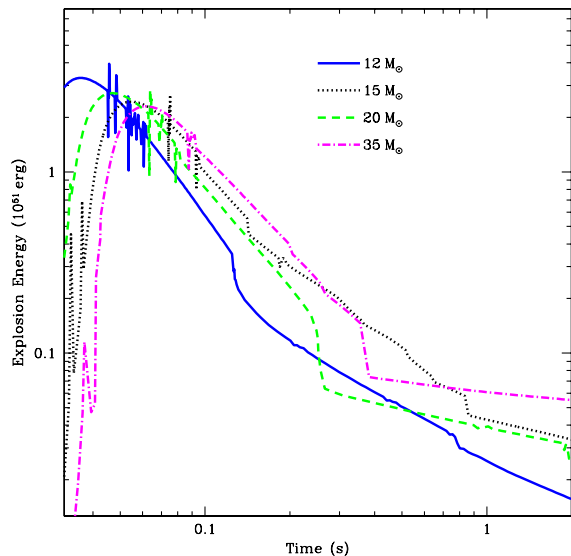


FIG. 8. Explosion energy as a function of time for 3 different progenitors. Here we have assumed that the explosion energy is dominated by the the energy stored in the convective region at the time of the launch of the explosion. The energy stored depends upon the rate of infall onto the the convection region. This infall acts as a pressure-cooker lid, stronger lids (with higher infall rates) can store more energy in the convection region (see[96, 98] for details).

mass distribution of neutron stars and black holes in binaries and compare them to the observed remnant mass distribution (Fig 9[97]). Current studies argue that if a gap exists in the remnant mass distribution, delayed explosions are rare, meaning that most collapsing stars either explode quickly and strongly or fail (or are extremely weak). If true, this result assures us that the neutrino signal from stellar collapse will cleanly probe nuclear and neutrino physics and not be significantly hampered by late-time explosion evolution or fallback.

This picture depends both on our understanding of the observations (which may stay have biases) and theory. We have already discussed the observational uncertainties. An alternate way to measure compact remnant masses is through gravitational wave observations of the merger of two compact remnants. As two compact remnants merge, they produce a strong gravitational wave signal. Compact mergers are expected to be the primary gravitational wave source for the advanced LIGO detector with a predicted rate of a few to one hundred detections per year when the detector is at full operations[99, 100]. To leading order, the phasing of the gravitational wave signal from these mergers depends upon the chirp mass of the binary: $\mu = (m_1 m_2)^{3/5} (m_1 + m_2)^{-1/5}$, where m_1 and m_2 are the masses of the two compact remnant masses in the binary. Higher order terms in the signal rely on mass ratios and, in principle, the masses of both compact remnants could

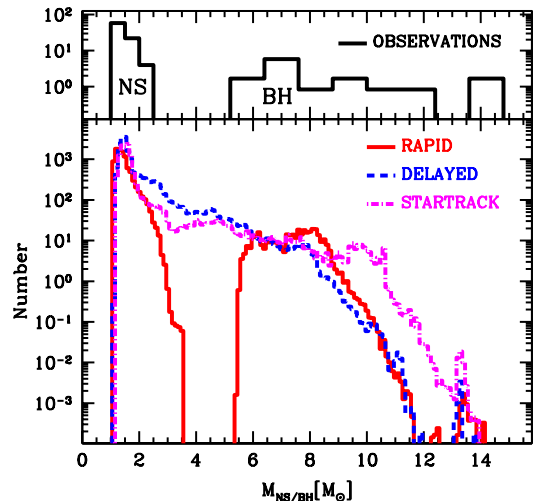


FIG. 9. Predicted neutron star/black hole mass distribution for the Galactic population of Roche lobe overflow and wind fed X-ray binaries. This result employed a population synthesis method to generate the binaries with two supernova explosion models. In the model in which the explosion is driven on a rapid timescale, we note the same striking gap in remnant mass (almost no compact objects in the gap region) as found in the observations. In contrast, the model in which the supernova explosion is significantly delayed shows a continuous compact object mass distribution. For comparison, we also show the remnant mass distribution commonly used in modern studies of Galactic and extra-galactic binaries with compact objects (see[97] for details.)

be determined from a strong gravitational wave detection. However, in practice, it is difficult to obtain exact masses with the typical signal expected with advanced LIGO[101]. Nonetheless, these detections should be able to provide independent information on the mass gap.

For our theoretical interpretation, we have made a series of assumptions. First, we have assumed that the explosion energy is stored in the convective region. If another energy source, for example rotational energy in the core, can be tapped, estimates using only the energy in the convective region underestimate the total explosion energy. These additional energy sources might make it that a delayed explosion can still produce a mass gap. We will have to use other means (supernova light curves) to determine whether such additional energy sources are present in the explosion. Other theoretical errors include our understanding of fallback. We will discuss this further in section IX.

VII. SUPERNOVA REMNANT EJECTA

The term supernova remnant is also used to refer to the interaction of the ejecta from the supernova explosion with the surrounding circumstellar medium. A series of analytic derivations are used to estimate the explosion energy, stellar structure, and the nature of the interstellar medium using supernova remnants[102, 103]. For most remnants, these estimates provide a first estimate of the initial supernova conditions. However, these analytic derivations tend to simplify the physics too much to be used to strongly constrain the supernova engine. In addition, supernova remnants are observed well after the actual supernova event and, for the most part, ejecta remnant observations can not be easily coupled with the other diagnostics of supernovae (the light-echo observation of the supernova outburst for the Cassiopeia A remnant being the one counter-example[104]). But supernova ejecta remnants provide insight into the explosion mechanism not detected by other diagnostic probes and despite the limitations of these observations, ejecta remnants remain powerful probes in our understanding of supernovae.

Until recently, most of the studies of supernova remnants have focused on hydrodynamics[105, 106] and particle acceleration[107–111], for a review, see[112]. With advent of spatially resolved cosmic ray detectors observations of supernova remnants(e.g.[113, 114]), studies of particle acceleration have intensified (e.g. [115–118]). Coupled with the wealth of observations from radio (e.g. VLBA) through gamma-rays (e.g. Fermi, HESS[119]), we are building a strong picture of particle acceleration processes. Studies of hydrodynamics have also taken advantage of the growing, time-resolved data from the Chandra satellite (e.g.[120]) of the development of instabilities and the ability to calculate these instabilities in 3-dimensions[121, 122]. With detailed models and a growing understanding of the initial conditions (see below), this wealth of data provides an ideal setting to study turbulence models.

Recent work, both observational and theoretical, has shown the potential of the supernova remnant as a powerful diagnostic tool to study the supernova explosion mechanism. Here we focus on one of the best-studied remnants: the Cassiopeia A supernova remnant.

First we review the theoretical advances in modeling the Cassiopeia A supernova remnant. Progenitor estimates for Cassiopeia A have ranged from a $16 M_{\odot}$ single star[123] to a very massive progenitor $30\text{--}60 M_{\odot}$ [124]. These efforts based their conclusions using stellar models in the literature. Recently, theorists have modeled Cassiopeia A progenitors, focusing on the constraints placed by it observations. This includes not only the shock position and velocity, but the nucleosynthetic yields and the presence of nitrogen-rich knots (allowing stellar modellers to predict that most of the hydrogen was removed prior to collapse, but most of the helium core must be retained)[125].

The observational study of Cassiopeia A extends across many decades in energy. The rapidly moving infra-red features in the region surrounding Cassiopeia A have been interpreted by observers as the light echo from the supernova explosion (whose light originally arrived to Earth 330 years ago) that formed the Cassiopeia A remnant[104]. With this interpretation, we now have an integrated spectrum of this supernovae that can also place constraints on its progenitor as that of a core-collapse Type IIb supernova with characteristics similar to that of SN 1993J.

Cassiopeia A also demonstrates the danger in over-interpreting the spatial distribution of the remnant ejecta seen in soft X-rays by chandra and XMM. Until the launch of the NuSTAR (Nuclear Spectroscopic Telescope Array) satellite[68], our view of remnants was limited to the material that is currently shocked to sufficient temperatures to be observed. For Cassiopeia A, maps of this shocked gas (Figure 10) argued both for a highly asymmetric (almost jet-like) explosion where somehow the iron was mixed out extensively (beyond the silicon layer). However, the NuSTAR satellite opened up a new window into studying these remnants. The 3-80keV bandwidth of NuSTAR includes the 67.86 and 78.36 keV lines produced in the decay of ^{44}Ti , producing a map of all the ^{44}Ti produced in the supernova shock, not just the shocked ^{44}Ti . Because ^{44}Ti is primarily produced with the same inner ejecta where ^{56}Ni (which decays to iron) is produced, these direct observations of ^{44}Ti provide an ideal tracers of the inner engine. The NuSTAR observations (Figure 10) demonstrate just how misleading shock-limited observations of remnant ejecta can be: unless some unknown mechanism decouples the ^{44}Ti and ^{56}Ni spatial distributions, most of the iron in Cassiopeia A remains unshocked and hidden. The puzzle of the bizarre iron distribution in Cassiopeia A was simply caused by only the shocked material. With NuSTAR, we not only construct a picture of a “normal” supernova, but we might have the first real evidence that the low-mode supernova engine model (either caused by low-mode Rayleigh-Taylor convection or advective-acoustic instabilities) is behind the Cassiopeia A explosion.

Observations of ^{44}Ti open up a new realm in studying nucleosynthetic yields and nuclear physics in supernovae. ^{44}Ti is produced primarily by material shocked to near NSE temperatures ($> 4 - 5 \times 10^9\text{K}$). But the exact amount of ^{44}Ti produced depends sensitively on the conditions of the material as it expands and cools. Indeed, even the way the ^{44}Ti is produced changes depending on the exact details[127]. An in depth review of these paths (identifying 4 distinct paths), and their dependence on the uncertainties in nuclear cross-sections exists[127] and we will simply summarize some of the critical points here. The separate paths include high density regions where the interaction rate for α particles is so high that very little helium is left in the final distribution after expansion. In these conditions, quasi-statistical equilibrium values provide an accurate description of the final yields

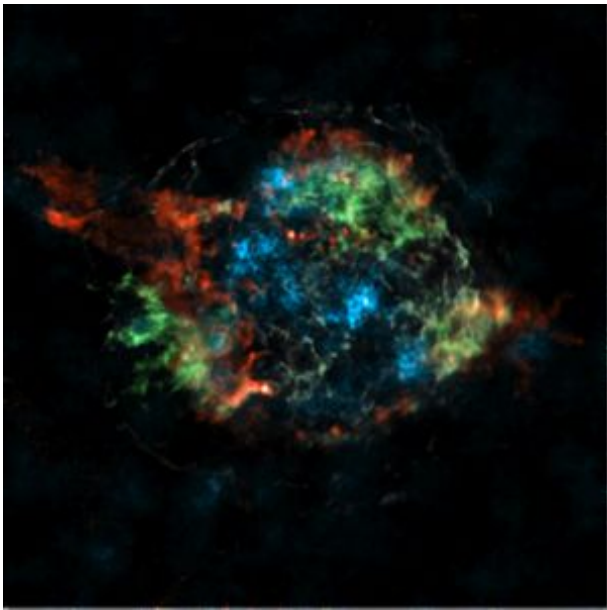


FIG. 10. A image showing a composite of the continuum (red), iron line emission (green) and ^{44}Ti -decay line distribution for the Cassiopeia A supernova remnant[126].

and these yields are primarily dependent on masses and Q-values. At lower densities, the isotopes cluster and the Si-Ca cluster (where ^{44}Ti lies) flows into the iron-peak, producing a chasm in ^{44}Ti production. Other regions probe peculiarities in the α -rich freeze-out.

Observing the distribution of ^{44}Ti yields and coupled with our understanding of nuclear reaction rates, we can probe the exact details of the supernova engine. For example, the chasm in ^{44}Ti yield is sensitive to details in the nuclear cross-sections. Figure 11 shows the titanium yield for a grid of temperatures and densities at peak temperature. The chasm is quite narrow as it moves up in density and temperature until it the temperature reaches $6 \times 10^9\text{K}$, where it then broadens and extends to a temperature of 10^{10}K at a density of a few times 10^8gcm^{-3} . The actual density where the chasm flattens out depends upon details in the nuclear physics. On top of this plot are the particles from a series of supernova explosions. In particular, note that the the data from the 1-dimensional Cassiopeia A explosions model lies right near the chasm. In such scenarios, the final ^{44}Ti yield is extremely sensitive to the nuclear physics determining th position of the chasm. If we had other constraints on the explosion trajectories, the ^{44}Ti yield becomes a strong nuclear physics probe.

The ejecta remnants of supernovae are ideally suited to probing nucleosynthetic yields. These yields can be used to both study nuclear reaction rates as well as better constrain the supernova engine. In particular, ejecta remnants have the potential to provide strong constraints on the asymmetry in the supernova explosion. Unfortunately, in most cases, we will not be able to combine disparate observations to place strong constraints on the su-

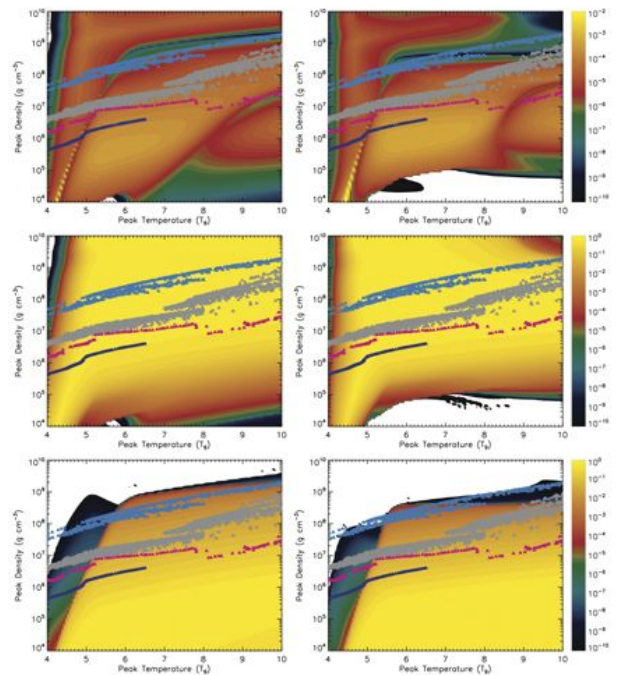


FIG. 11. Final mass fraction of ^{44}Ti (first row), ^{56}Ni (second row), and ^4He (third row) in the peak temperature-density plane. The left column assumes an exponential decay evolution for the density and temperature evolution with time whereas the right column assumes a power-law pevolution profile[127]. The different colored triangles refer to the trajectories of different supernova and hypernova explosion models - blue for a one-dimensional Cassiopeia A model[125], gray for the two-dimensional explosion of rotating progenitor E15B[128], pink for a one-dimensional hypernova model[129] and cyan for a two-dimensional magnetohydrodynamic collapsar model. The exact location of the valley in ^{44}Ti production is extremely sensitive to the details in the nuclear physics.

pernova explosion, with the exception of a few examples such as Casseiopeia A (where we can observe the light-echo supernova) or SN 1987A (which is young enough and near enough to us so that the next generation of imaging hard X-ray satellites will resolve the quickly growing SN 1987A remnant). But ejecta remnant observations alone will still provide insight into the asymmetries and nucleosynthesis in supernovae that can be incorporated into our current understanding of supernova explosions.

VIII. NUCLEOSYNTHETIC YIELDS: STARS AND METEORITES

Nucleosynthetic yields of key elements like ^{56}Ni and ^{44}Ti can be measured in individual supernovae in the outburst itself or in the late-time supernova remnant, but more detailed yields are typically observed only in an integrated sense, either in stars after the supernova ejecta has been swept up in a new burst of star formation

or in meteorites. Although these observations are limited to integrated yields that might include components from multiple supernovae, they have been extensively used to constrain our understanding of the supernova explosion. Here we review just a few examples of this diagnostic is used in practice.

Extremely metal poor stars are ideal probes of the nucleosynthetic yields of the first high-mass, zero metallicity stars. Produced in the early universe, these low-mass stars that survive to the present day are being observed with increasing frequency. The first surveys showed the success of such work in the early 80s and 90s[130–132], but new surveys have rapidly accelerated this work (e.g.[133–136]). A wide variety of surveys (to name a few, SDSS/SEGUE[133], APOGEE[134], LAMOST[137]) are being conducted or planned that will increase this data significantly in the next decade. Astronomers can also use abundance patterns in damped Ly α systems to study the nucleosynthetic yields of the early universe[138]. These studies, focusing on the second generation of stars, have the advantage that they are not contaminated by too many supernova explosions.

Studying the yields of the earliest stars can provide insight into the first generation of stars and their formation. This first generation of star formation might produce a more exotic set of stars that can provide deeper insight into stellar evolution and supernovae (e.g. pair-instability supernovae). The explosions of these systems make firm predictions on the relative abundances of odd and even- Z elements[139, 140] and observations of this odd-even effect[138, 141] could provide deep insight into stellar evolution.

The origin of the r-process is another feature of supernovae that has been studied using abundance patterns in low-metallicity stars. With these observations, scientists have argued that at least some of the r-process must be produced in massive stars[142] and scientists have gone so far as to use these observations to justify particular r-process sites[143, 144]. Although there is still quite a bit of uncertainty in these observations, these constraints will ultimately tell us about both the supernova progenitor and its subsequent explosion. We will discuss this in more detail in section IX.

For high- z elements, it becomes difficult to determine the relative isotopic abundances in the spectra as the line differences become difficult to distinguish. However, in meteoritic data, the relative isotopic abundances can be determined (for a review, see[145]). These isotopic abundances can be used to constrain new nuclear/neutrino physics abundances. For example, neutrinos can alter the nucleosynthetic yields of supernovae. Neutrinos can excite elements, even unbinding some of the particles. The evaporation of a neutron or proton can lead to new nucleosynthetic paths, altering these final yields. This so-called “ ν -process”[146] can produce rare isotopes that are potentially detectable in both stellar and meteoritic data. For example, the ratio of ^{92}Nb to ^{93}Nb has been measured using solar system meteorites[147]

Because the nucleosynthetic yields are typically integrated results, what we learn from them depends heavily on our theoretical understanding of both the supernova engine and nuclear physics. We must use all of our diagnostics to help constrain the physics behind supernovae before we can truly take advantage of the integrated nucleosynthetic yields. But with a basic theoretical understanding calibrated by our other diagnostics, we can use these yields to place strong constraints on nuclear burning rates and the origin of the heavy elements.

IX. TYING MULTIPLE CONSTRAINTS TOGETHER, POST-EXPLOSION NUCLEOSYNTHESIS

Understanding the r-process is an example of how multiple diagnostics can be used together in concert with theory to study a physical process. The origin of the r-process elements remains one of the great unsolved problems of nuclear astrophysics with many production sites with neutron star mergers[148] and core-collapse supernovae[149] being dominant sources. Although it is possible that the merger of two neutron stars may be the dominant source of the r-process, it is likely that core-collapse supernovae play some role in the production of these heavy elements. After the launch of the explosion, neutrinos leak out of the neutron star, driving a neutron-rich wind. Neutron capture in this wind can build up extremely heavy elements, and the neutrino-driven wind mechanism has long been considered a prime site for r-process nucleosynthesis. Post-explosion nucleosynthesis focuses on the nucleosynthetic yields from this cooling neutron star.

The basic neutrino-drive wind r-process model argues that the high neutrino flux of the cooling neutron star ejects the outer layer of the neutron star (the ejecta mass need only be $10^{-6} M_{\odot}$ to explain r-process yields)[149–154]. The anti-electron neutrinos are typically higher-energy than the electron neutrinos and hence have a higher cross-section with the wind matter. This preserves the neutron-rich nature of this ejecta and rapid neutron capture produces the r-process. The high entropies, fast expansion, and neutron richness of this wind ejecta may provide the right conditions for making r-process nuclei[154]. However, current calculations suggest that the basic model for neutrino-driven wind r-process only works in extreme conditions (e.g., $>2 M_{\odot}$ neutron stars[143, 156], for a review, see[155]).

A number of solutions have been proposed, including magnetic fields that can alter the wind trajectories, providing time for sufficient neutron captures and decays to produce the r-process[156, 157]. But most of the detailed physics work has focused on the role nuclear physics might play in “fixing” the neutrino-driven wind site for r-process. Unfortunately, self-consistent studies including neutrino capture reactions into a reaction network code have shown that that the interplay between neutrino

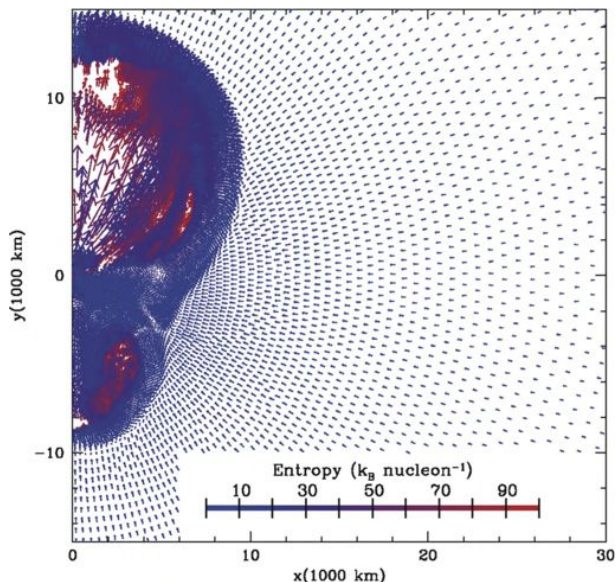


FIG. 12. A snapshot in time of a 2-dimensional fallback accretion model (the neutron star is at the 0,0 point). The arrows denote the direction of the velocity and the outflow can be seen along the y axis. Colors denote entropy and the entropy of the ejecta can be very high entropy[164].

and nuclear reactions, if anything, makes it more difficult to produce the r-process[158–160]. Neutrino oscillations (including active-sterile neutrino conversion) have been proposed as a nuclear-physics solution fixing the neutrino-driven r-process scenario[161, 162]. The uncertainties in the nuclear mass models still can change this picture dramatically[163]. With the development of the Facility for Rare Isotope Beams (FRIB), this physics uncertainty may be removed, strengthening the studies of neutrino physics.

An alternate solution invokes the fallback of material after the launch of the explosion. Fallback material crashes back down onto the proto-neutron star, providing a new source of neutrinos and heat. Some (up to 25%) of this material can be ejected[164]. Figure 12 is a snapshot in time during this fallback, showing the outflowing ejecta. Much of the re-ejected material is not neutron rich and typically produces iron-peak elements. This ejecta provides a second source of ^{56}Ni to help power supernova light-curves. Since most of the fallback occurs in the first 100s, this new ejecta becomes part of the supernova explosion when the shock breaks out of the star. The energy from this fallback ejecta, especially late-time fallback, has been used to explain a variety of peculiar supernovae[165].

The yield of this ejecta is highly sensitive to the amount of free neutrons in the system. A 1% variation in the electron fraction can make the difference between a clear r-process signature (with an electron fraction of 0.495) and a strong iron peak yield (with an electron fraction of 0.505). The evolution of an r-process yield in this fallback scenario is very different than typical r-

process production sites. With the low neutron fraction of this scenario, the abundances stay near the valley of stability and proton capture is able to drive the element mass beyond waiting points. Only at late times do the protons freeze out, allowing the neutrons to develop a typical r-process isotope distribution. This nucleosynthetic path was termed “rpn-process” (rapid proton and neutron capture) in the first fallback study[164] and it is a variant of the i-process (intermediate process) heavy element nucleosynthesis. Because of the sensitivity to the exact number of neutron and proton fractions, this site is sensitive to the hydrodynamics, neutrino processes and nuclear reaction rates and much more must be studied to understand it better.

To test this model, we can compare our r-process signature to the observed signature in stars or meteorites (see Sec.VIII). If we trust our fallback model implicitly, we can use these yields to constrain the nuclear physics governing these yields. Independent validation of our fallback models is needed to provide that trust. Of course, the neutrino signal will measure this late-time fallback. But we can also utilize the data on compact remnants and supernova light curves to validate our fallback model. Let’s review this validation data in more detail.

Because current explosive engine calculations are still sensitive to broad range of details (see Hix review), we can not hope to cover the possible range of explosion features to conduct a complete study of fallback. Instead, most calculations implement artificially the explosion energy. Unfortunately, how this energy is injected can drastically alter the amount and timing of the fallback. Models driven by pistons tend to produce late time fallback whereas the arguably more physically-relevant energy driven explosions produce fallback almost immediately[166]. Figure 13 shows the fallback rates estimated for 3 different progenitors and a range of explosion energies[31]. For these calculations, the fallback occurs immediately. It is this fallback that produces the r-process yields, but only if there is considerable fallback. We can use studies of compact remnant masses to get a handle on the amount of fallback in typical supernovae. The amount of systems that form remnant masses above $1.4\text{--}1.5M_{\odot}$ provides us with a rough estimate of how many systems are likely to have more than a few tenths of a solar mass of fallback. Comparing these results to our fallback models can determine the rate at which supernovae can produce r-process from fallback.

We can also try to use supernova light-curves to constrain fallback. With a supernova light-curve, we can estimate the explosion energy and the role the fallback accretion plays in the light-curve. If we can see evidence of the fallback in the light-curve, we will be able to place constraints on the nature of the fallback. Unfortunately, although fallback has been argued to explain some peculiar supernovae[165], the fact that alternation explanations exist for these supernovae make it difficult to use this as a constraint. However, if we can produced an unbiased fraction of weak supernovae (with little ^{56}Ni

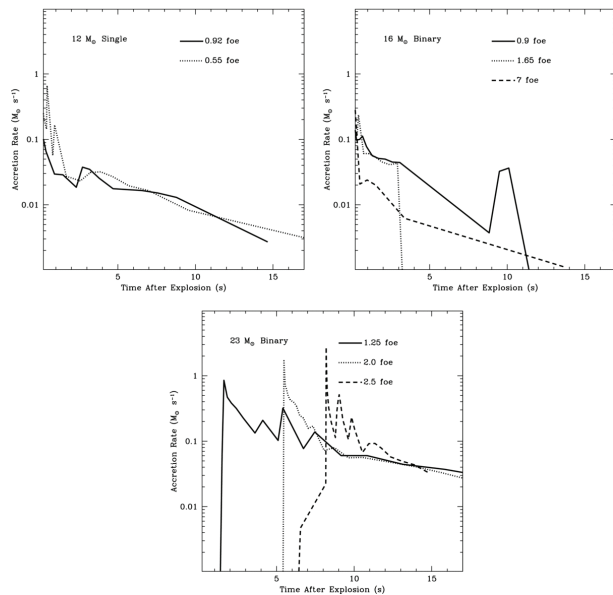


FIG. 13. The fallback accretion rate for 3 different progenitors each with different explosion energies[31]. The accretion stars nearly immediately after the launch of the explosion. Indeed, in many core-collapse engine models, this fallback can be seen while the shock moves outward.

yield), the fraction can be used to better understand fallback. Coupled with the remnant mass distribution, these observations will be able to distinguish between early and late-time fallback mechanisms.

With a neutrino detection following the fallback, we will be able to strongly constrain the fallback and for nearby supernovae where all of our diagnostics are available, we should be able to make strong predictions on the total amount of fallback and its timing.

X. SUMMARY

Supernovae are indeed Nature’s laboratories for matter in extreme conditions. Traditional studies of this extreme physics have focused on the neutrino and gravitational wave diagnostics of supernovae. But nearly all the data we have on supernovae used different diagnostics. In this review, we have discussed the range of diagnostics: neutrinos, gravitational waves, progenitor studies, the supernova outbursts (a wide range of photon energies), compact remnant mass distributions, ejecta remnant observations, and integrated nucleosynthetic yield constraints from low-metallicity stars and meteoritics.

All of these diagnostics have strengths and weaknesses, but taken together, we are at the stage of truly constraining nuclear and particle physics with our supernova “experiment”. Some of these diagnostics require considerable theory work to interpret and any study of supernovae as physics laboratories will require a strong theoretical understanding. The wealth of data will be able to both help us understand the uncertainties in this theoretical understanding as well as provide constraints on our errors in studying nuclear physics.

Supernova studies are at a critical point where new surveys and new observational experiments will soon drastically increase the amount of data. Along with advances in our theoretical understanding, we are on the cusp of a revolution in this science and it is likely that the next decade will see large breakthroughs in this science.

ACKNOWLEDGMENTS

The work of C.L.F. and W.E. was done under the auspices of the National Nuclear Security Administration of the U.S. Department of Energy at Los Alamos National Laboratory under Contract DE-AC52-06NA25396.

-
- [1] Abrahamyan, S. et al., *Phys. Rev. Lett.*, **108**, 112502 (2012)
 - [2] Baron, E., Bethe, H.A., Brown, G.E., Cooperstein, J., Kahana, S. *Phys. Rev. Lett.*, **59**, 736 (1987)
 - [3] Herwig, F., *ARA&A*, **43**, 435 (2005)
 - [4] Herant, M., Benz, W., Hix, W.R., Fryer, C.L., Colgate, S.A. *ApJ*, **435**, 339
 - [5] Blondin, J.M., Mezzacappa, A., DeMarino, C., *ApJ*, **584**, 971 (2003)
 - [6] Foglizzo, T., Galletti, P., Scheck, L., Janka, H.-Th., *ApJ*, **654**, 1006 (2007)
 - [7] de Gouvêa, A., et al. *hep-ex/1310.4340*, (2013)
 - [8] Alimonti, G., et al., *Nucl. Instrum. Meth.*, **A600**, 568 (2009)
 - [9] Mitsui, T. et al., *Nucl. Phys. Proc. Suppl*, **221**, 193 (2011)
 - [10] Kraus, C. and Peeters, S.J.M. et al., *Prog. Part. Nuc. Phys.*, **64**, 273 (2010)
 - [11] Balantekin, A.B. et al., *astro-ph/1307.7419*
 - [12] Maricic, J. et al., *Nucl. Phys. Proc. Suppl*, **221**, 173 (2011)
 - [13] Wurm, M. et al., *Journ. Astroparticl Phys.*, **11**, 685 (2012)
 - [14] Abe, K. et al., *Phys. Rev. D*, **83**, 052010 (2011)
 - [15] Aharmim, B. et al., *Phys. Rev. C*, **88**, 025501 (2013)
 - [16] Roberts, L.F., Reddy, S., Shen, G. *Phys. Rev. C*, **86**, 065803 (2012)
 - [17] Martínez-Pinedo, G. Fischer, T., Lohs, a., Huther, L. *Phys. Rev. Lett.*, **109**, 251104 (2012)
 - [18] Roberts, L.F., Shen, G., Cirigliano, V., Pons, J.A., Reddy, S., Woosley, S.E. *Phys. Rev. Lett.*, **108**, 061103 (2012)
 - [19] Reddy, S., Prakash, M., Lattimer, J.M. *Phys. Rev. D*, **58**, 013009 (2012)
 - [20] Duan, H. Fuller, G. M. and Qian, Y.-Z. *Phys.Rev.* **D74**, 123004 (2006).
 - [21] Fogli, G. L., Lisi, E. Marrone, A., and Mirizzi, A. *JCAP*, **0712**, 010 (2007).

- [22] Raffelt, G. G. and Smirnov A. Y. *Phys.Rev.* **D76**, 081301 (2007)
- [23] Raffelt, G. G. and Smirnov A. Y. *Phys.Rev.* **D76**, 125008 (2007)
- [24] Esteban-Pretel, A. Mirizzi, A., Pastor, S., Tomas, R., Raffelt, G.G., et al. *Phys.Rev.* **D78**, 085012 (2008)
- [25] Duan, H. and Kneller, J. P. *J.Phys. G* **G36**, 113201 (2009)
- [26] Dasgupta, B., Dighe, A., Raffelt, G. G., and Smirnov, A. Yu. *Phys.Rev.Lett.*, **103**, 051105 (2009).
- [27] Duan, H. , Fuller, G. M., and Qian, Y.-Z., *Ann.Rev.Nucl.Part.Sci.* **60**, 569 (2010)
- [28] Duan, H. and Friedland, A. *Phys.Rev.Lett.* **106**, 091101 (2011)
- [29] Duan, H. and Friedland, A., McLaughlin, G.C., Surman, R. *J. phys. G* **G38**, 035201 (2011)
- [30] Borriello, E., Chakraborty, S., Janka, H.-T., Eligio, L., Mirizzi, A., *astro-ph/1310.7488*
- [31] Fryer, C.L. *ApJ*, **699**, 409 (2009)
- [32] Price, L. et al. *HEAD* **13**, 121.02 (2013)
- [33] Aso, Y. et al. *Phys. Rev. D* **88**, 043007 (2013)
- [34] Fryer, C.L., New, K.C.B., *Living Reviews in Relativity*, **14**, 1 (2011)
- [35] Fryer, C.L., Holz, D.E., Hughes, S.A., *ApJ*, **565**, 430 (2004)
- [36] Fryer, C.L., Holz, D.E., Hughes, S.A., *ApJ*, **609**, 288 (2004)
- [37] Murphy, J.W., Ott, C.D., Burrows, A. *ApJ*, **707**, 1173 (2009)
- [38] Fryer, C.L., Young, P.A. *ApJ*, **659**, 1438 (2007)
- [39] Cappellaro, E.; Evans, R.; Turatto, M. *A&A*, **351**, 459 (1999)
- [40] van den Bergh, S. Li, W., Filippenko, A. V. *PASP*, **117**, 773 (2005)
- [41] Li, W., Wang, X., Van Dyk, S. D., Cuillandre, J.-C., Foley, R. J.; Filippenko, A. V. *ApJ*, **661**, 1013 (2007)
- [42] Smartt, S.J., Eldridge, J.J., Crockett, R.M., Maund, J.R. *MNRAS*, **395**, 1409 (2009b)
- [43] Smartt, S.J. *ARA&A*, **47**, 63 (2009a)
- [44] Anderson, J.P., Habergham, S.M., James, P.A., Hamuy, M. *IAUS*, **279**, 183 (2012)
- [45] Kelly, P.L., Kirshner, R.P. *ApJ*, **759**, 107 (2012)
- [46] Fryer, C.L. et al. *PASP*, **119**, 1211 (2007)
- [47] Podsiadlowski, P., Joss, P. C., & Hsu, J. J. L. *ApJ*, **391**, 246 (1992)
- [48] Vanbeveren, D., Van Bever, J., Belkus, H. *ApJ*, **662**, L107 (2007)
- [49] Vanbeveren, D., Mennekens, N., Van Rensbergen, W., De Loore, C. *A&A*, **552**, 105 (2013)
- [50] Meynet, G., Georgy, C., Hirschi, R., Maeder, A., Massey, P., Przybilla, N., Nieva, M.-F. *Proceedings of the 39th Liege Astrophysical Colloquium, held in Liege 12-16 July 2010, edited by G. Rauw, M. De Becker, Y. Naze, J.-M. Vreux, P. Williams*, **80**, 266 (2011)
- [51] Kiminki, D.C. et al. *ApJ*, **664**, 1102 (2007)
- [52] Kobulnicky, H.A., Fryer, C.L. *ApJ*, **670**, 747 (2008)
- [53] Kiminki, D.C., Kobulnicky, H.A. *ApJ*, **751**, 4 (2012)
- [54] Podsiadlowski, P. *Space Science Rev.*, **66**, 439 (1993)
- [55] Maund, J.R., Mattila, S., Ramirez-Ruiz, E., Eldridge, J.J., *astro-ph/1308.4393* (2013)
- [56] Crockett, R.M., Eldridge, J.J., Smartt, S.J., Pastorello, A., Gal-Yam, A., Fox, D.B., Leonard, D.C., Kasliwal, M.M., Mattila, S., Maund, J.R., Stephens, A.W., Danziger, I.J., *MNRAS*, **391**, L5 (2008)
- [57] Elias-Rosa, N., Van Dyk, S.D., Li, W., Morell, N., Gonzalez, S., Hamuy, M., Filippenko, A.V., Cuillandre, J.-C., Foley, R.J., Smith, N., *ApJ*, **706**, 1174 (2009)
- [58] Fraser, M. et al., *MNRAS*, **417**, 1417 (2011)
- [59] Van Dyk, S. D. et al., *ApJ*, **741**, L28 (2011)
- [60] Szczygiel, D.M., Gerke, J.R., Kochanek, C.S., Stanek, K.Z., *ApJ*, **747**, 23 (2012)
- [61] Van Dyk, S. D. et al., *ApJ*, **772**, L32 (2013)
- [62] Van Dyk, S. D. et al., *ApJ*, **756**, 131 (2012)
- [63] Cao, Y. et al., *ApJ*, **775**, L7 (2013)
- [64] Groh, J.H., Georgy, C., Ekström, S., *A&A*, **558**, L1 (2013)
- [65] Fryer, C.L., *ApJ*, **522**, 413 (1999)
- [66] Heger, A., Fryer, C.L., Woosley, S.E., Langer, N., Hartmann, D.H., *ApJ*, **591**, 288 (2003)
- [67] Gehrels, N. et al. *ApJ*, **611**, 1005 (2004)
- [68] Harrison, F.A. et al. *ApJ*, **770**, 103, (2013)
- [69] Fryer, C.L., Hungerford, A.L., Young, P.A. *ApJ*, **662**, L55 (2007c)
- [70] Bayless, A.J., Even, W., Frey, L.H., Fryer, C.L., Roming, P.W.A., Young, P.A. *astro-ph/1401.4449*, (2014)
- [71] Ofek, E.O. et al. *astro-ph/1307.2247*, (2013)
- [72] Blinnikov, S.I., Bartunov, O.S. *A&A*, **273**, 106, (1993)
- [73] Frey, L, Even, W., Whalen, D.J., Fryer, C.L., Hungerford, A.L., Fontes, C.J., Colgan, J. *ApJS*, **204**, 16, (2013)
- [74] Maeda, K., Mazali, P.A., Nomoto, K. *ApJ*, **645**, 1331, (2006)
- [75] Kasen, D., Thomas, R.C., Röpke, F., Woosley, S.E. *Journ. Phys. Conf. Ser.*, **125**, 2007, (2008)
- [76] Mazzali, P.A., Lucy, L.B. *A&A*, **279**, 447 (1993)
- [77] Remington, B.A., Drake, R.P., Ryutov, D.D. *Rev. Mod. Phys.*, **78**, 755 (2006)
- [78] Demorest, P.B., Penucci, T., Ransom, S.M, Roberts, M.S.E., Hessels, J.W.T. *Nature*, **467**, 1081 (2010)
- [79] Hebel, J.M., Lattimer, J.M., Pethick, C.J., Schwenk, A. *ApJ*, **773**, 11 (2013)
- [80] Finn, L. S. *PRL*, **73**, 1878 (1994)
- [81] Bailyn, C.D., Jain, R.K., Coppi, P., & Orosz, J.A. *ApJ*, **499**, 367 (1998)
- [82] Thorsett, S.E., & Chakrabarty, D. *ApJ*, **512**, 288 (1999)
- [83] Özel, F., Psaltis, D., Narayan, R. & McClintock, J.E. *ApJ*, **725**, 1918 (2010)
- [84] Farr, W.M., et al. *ApJ*, **741**, 103 (2011)
- [85] Özel, F., Psaltis, D., Narayan, R. & Santos, V. *ApJ*, **757**, 55 (2012)
- [86] Kreidberg, L., Bailyn, C.D., Farr, W.M, & Kalogera, V. *ApJ*, **757**, 36 (2012)
- [87] Willems, B., Henninger, M., Levin, T., Ivanova, N., Kalogera, V., McGhee, K., Timmes, F.X., Fryer, C.L. *ApJ*, **625**, 324 (2005)
- [88] Fragos, T., Willems, B., Kalogera, V., Ivanova, N., Rockefeller, G., Fryer, C.L., Young, P.A. *ApJ*, **697**, 1057 (2009)
- [89] Burrows, A., Hayes, J., Fryxell, B.A. *ApJ*, **450**, 830 (1995)
- [90] Janka, H.-T., Mueller, E. *A&A*, **306**, 167 (1996)
- [91] Fryer, C.L., Warren, M.S. *ApJ*, **574** L65 (2002)
- [92] Fryer, C.L., Warren, M.S. *ApJ*, **601** 391 (2004)
- [93] Blondin, J.M., Mezzacappa, A. *ApJ*, **642** 401 (2006)
- [94] Bruenn, S.W., Mezzacappa, A., Hix, W.R., Blondin, J.M., Marronetti, P., Messer, O.E.B., Dirck, C.J.,

- Yoshida, S. *Jour. Phys. Conf. Ser.*, **180**, 2018 (2009)
- [95] Hanke, F., Müller, B., Wongwathanarat, A., Marek, A., Janka, H.-T. *ApJ*, **770** 66 (2013)
- [96] Fryer, C.L., Belczynski, K., Wiktorowicz, G., Dominik, M., Kalogera, V., Holz, D.E. *ApJ*, **749** 91 (2012)
- [97] Belczynski, K., Wiktorowicz, G., Fryer, C.L., Holz, D.E., Kalogera, V. *ApJ*, **757** 91 (2012)
- [98] Fryer, C.L., *New Astron.*, **50**, 492 (2006a)
- [99] Abadie, J., et al. *Class. Quant. Gravity*, **27**, 173001 (2010)
- [100] Dominik, M., et al. *ApJ*, **759**, 52 (2012)
- [101] Hannam, M., Brown, D.A., Fairhurst, S., Fryer, C.L., Harry, I.W. *ApJ*, **766**, L14
- [102] Chevalier, R.A. *ApJ*, **258**, 790 (1982a)
- [103] Chevalier, R.A. *ApJ*, **259**, 302 (1982b)
- [104] Krause, O. et al. *Science*, **308**, 1604 (2005)
- [105] Chevalier, R.A., Blondin, J.M., Emmering, R.T., *ApJ*, **444**, 312 (1992)
- [106] Blondin, J.M., Lundqvist, P., Chevalier, R.A. *ApJ*, **472**, 257 (1996)
- [107] Blandford, R.D., Ostriker, J.P. *ApJ*, **221**, L29 (1978)
- [108] Bell, A.R. *MNRAS*, **182**, 147 (1978a)
- [109] Bell, A.R. *MNRAS*, **182**, 443 (1978b)
- [110] Jones, F.C., Ellison, D.C. *Space Science Rev.*, **58**, 259 (1991)
- [111] Ellison, D.C., Berezhko, E.G., Baring, M.G. *ApJ*, **540**, 292 (2000)
- [112] Reynolds, S.P. *ARA&A*, **46**, 89 (2008)
- [113] Aharonian, F. et al. *A&A*, **437**, L7 (2005)
- [114] Aliu, E. et al., *ApJ*, **770**, 93 (2013)
- [115] Yuan, Q., Liu, S., Fan, Z., Bi, X., Fryer, C.L. *ApJ*, **735**, 120 (2011)
- [116] Telezhinsky, I., Dwarkadas, V.V., Pohl, M. *A&A*, **552**, 102 (2013)
- [117] Morlino, G., blasi, P., Bandiera, R., Amato, E., Caprioli, D. *ApJ*, **768**, 179 (2013)
- [118] Bykov, A.M., Malkov, M.A., Raymond, J.C., Krasichichtchikov, A.M., Valdimirov, A.E. *Space Sci. Rev.*, **178**, 599 (2013)
- [119] Aharonian, F.A. *Astroparticle Phys.*, **43**, 71 (2013)
- [120] Hwang, U., Laming, J.M. *ApJ*, **746**, 130 (2012)
- [121] Obergaulinger, M., Iyudin, A.F., Müller, E., Smoot, G.F. *MNRAS*, **advanced access 18pp** (2013)
- [122] Ellinger, C.I., Rockefeller, G., Fryer, C.L., Young, P.A., Park, S. *astro-ph/1305.4137* (2013)
- [123] Chevalier, R.A., Oishi, J. *ApJ*, **593**, L23 (2003)
- [124] Fesen, R.A., Becker, R.H. *ApJ*, **371**, 621 (1991)
- [125] Young, P.A. et al. *ApJ*, **640**, 891 (2006)
- [126] Grefenstette, B. et al. *submitted to Nature*
- [127] Magkotsios, G., Timmes, F.X., Hungerford, A.L., Fryer, C.L., Young, P.A., Wiescher, M. *ApJS*, **191**, 66 (2010)
- [128] Fryer, C.L., & Heger, A. *ApJ*, **541**, 1033
- [129] Fryer, C.L., Young, P.A., & Hungerford, A.L. *ApJ*, **650**, 1028 (2006b)
- [130] Beers, T.C., Preston, G.W., & Shectman, S.A. *AJ*, **90**, 2089, (1985)
- [131] Ryan, S.G., Norris, J.E., & Bessell, M.S. *AJ*, **102**, 303, (1991)
- [132] Beers, T.C., Preston, G.W., & Shectman, S.A. *AJ*, **103**, 1987, (1992)
- [133] Aoki et al. *AJ*, **145**, 13, (2013)
- [134] García Pérez, A.E. et al. *ApJ*, **767**, L9, (2013)
- [135] Lee, Y.S. et al. *AJ*, **146**, 132, (2013)
- [136] Placco, V.M. *astro-ph/1311-5855*
- [137] Deng, L.-C., et al. *Research in Astronomy and Astrophysics*, **12**, 7 (2012)
- [138] Fenner, Y., Prochaska, J.X., Gibson, B.K. *ApJ*, **606**, 116
- [139] Nakamura, T., Umeda, H., Nomoto, K., Thielemann, F.-K., Burrows, A. *ApJ*, **517**, 193
- [140] Heger, A., Woosley, S.E. *ApJ*, **567**, 532 (2002)
- [141] Ryan, S.G., Norris, J.E., Beers, T.C. *ApJ*, **471**, 254 (1996)
- [142] Qian, Y.-Z., Wasserburg, G.J. *ApJ*, **567**, 515 (2002)
- [143] Argast, D., Samland, M., Thieleman, F.-K., Qian, Y.-Z. *A&A*, **416**, 997 (2004)
- [144] Qian, Y.-Z. *AIP Conf*, **87**, 5805 (2012)
- [145] Anders, E., Grevesse, N. *Geochimica et Cosmochimica Acta*, **53**, 197 (1989)
- [146] Woosley, S.E., Hartmann, D.H., Hoffman, R.D., Haxton, W.C. *ApJ*, **356**, 272 (1990)
- [147] Hayakawa, T., Nakamura, K., Kajino, T., Chiba, S., Iwamoto, N., Cheoun, M.K., Mathews, G. J. *ApJ*, **779**, L9 (2013)
- [148] Levinson, A., Eichler, D. *ApJ*, **418**, 386
- [149] Woosley, S.E., Hoffman, R.D. *ApJ*, **395**, 202 (1992)
- [150] Meyer, B.S., Mathews, G.J., Howard, W.M., Woosley, S.E., Hoffman, R.D. *ApJ*, **399**, 656 (1992)
- [151] Howard, W.M., Goriely, S., Rayet, M., Arnould, M. *ApJ*, **417**, 713 (1993)
- [152] Takahashi, K., Witt, J., Janka, H.-T. *A&A*, **286**, 857 (1994)
- [153] Woosley, S.E., Mathews, G.J., Wilson, J.R., Hoffman, R.D., Meyer, B.S. *ApJ*, **433**, 229 (1994)
- [154] Qian, Y.-Z., Woosley, S.E. *ApJ*, **471**, 331 (1996)
- [155] Thompson, T.A., Burrows, A., Meyer, B.S. *ApJ*. **562**, 887
- [156] Suzuki, T.K., & Nagataki, S. *ApJ*, **628**, 914 (2005)
- [157] Metzger, B.D., Thompson, T.A., Quataert, E. *ApJ*, **659**, 561 (2007)
- [158] Fuller, G.M., Meyer, B.S. *ApJ*, **453**, 792 (1995)
- [159] McLaughlin, G.C., Fuller, G.M., Wilson, J.R. *ApJ*, **472**, 440 (1996)
- [160] Meyer, B.S., McLaughlin, G.C., Fuller, G.M. *Phys. Rev. C*, **58**, 3698 (1998)
- [161] Fuller, G.M. *AIPC*, **412**, 160 (1997)
- [162] Fetter, J., McLaughlin, G.C., Balantekin, A.B., Fuller, G.M. *Astropart. Phys.*, **18**, 433 (2003)
- [163] Xu, X.D., Sun, B., Niu, Z.M., Li, Z., Qian, Y.-Z., Meng, J. *Phys. Rev. C*, **87**, 5805
- [164] Fryer, C.L., Herwig, F., Hungerford, A.L., Timemes, F.X. *ApJ*, **646**, L131 (2006c)
- [165] Dexter, J., Kasen, D. *ApJ*, **772**, 30 (2013)
- [166] Young, P.A., & Fryer, C.L. *ApJ*, **550**, 357 (2007)